Bull Eng Geol Environ (2015) 74:759–773
DOI 10.1007/s10064-014-0678-5

ORIGINAL PAPER

Shear strength properties of Dimitrovgrad flysch, Southeastern Serbia

Zoran Berisavljević · Dušan Berisavljević · Vladimir Čebašek

Received: 7 May 2014 / Accepted: 7 September 2014 / Published online: 1 October 2014

Abstract Flysch deposits are common in Serbia. Approximately 15 % of the 250 km of highways currently under construction will be constructed in flysch. In the most southern part of the E80 project, close to the border crossing with Bulgaria, construction of 3-km long cuts, often over 30 m high, is foreseen by the design. The geology of this part of Serbia is mainly characterized by flysch deposits represented by a sequence of sandstone and siltstone, interchanging in different proportions. After excavation of a majority of the cuts, several slopes suffered from global and structural instabilities. This required re-design of one part of the cuts. For this purpose, a geological strength index (GSI) was estimated and the structural features of rock discontinuities were observed on the faces of the surface excavations. This information and data obtained from laboratory testing enabled the determination of five characteristic rock mass types. For every type, shear strength properties were determined based on three criteria: the Hoek–Brown failure criterion; the Mohr–Coulomb criterion; and an hyperbolic nonlinear envelope. During the process of converting the Hoek–Brown parameters to the parameters of hyperbolic envelope, the Levenberg–Marquardt algorithm (LMA) was utilized to solve for the nonlinear regression problem. Verification of the parameters was performed on several examples. The median angle pressure increases exponentially with the GSI value and ranges between the value characteristic for clays and well-graded gravel. The maximum angle difference is obtained for a GSI value of 30. The average normal effective stress acting on the failed slopes, expressed in the form of the stress level ratio (SLR), is below 0.5. This indicates that the curved part of the shear strength envelope is utilized during the shearing. As such, the linear segment overestimates the shear strength.

Keywords Road cut · GSI · Shear strength · Nonlinear envelope

Z. Berisavljević (✉)
Sector for Technical Preparations and Designing,
Koridori Srbije Ltd., 21 Kralja Petra Street, 11000 Belgrade, Serbia
e-mail: z.berisavljevic@koridorisrbije.rs

D. Berisavljević
Center for Roads and Geotechnics, Institute for Material Testing,
Blvd. Vojvode Mišića 43, 11000 Belgrade, Serbia
e-mail: dusan.berisavljevic@institutims.rs

V. Čebašek
Faculty of Mining and Geology, University of Belgrade,
7 Đušina Street, 11000 Belgrade, Serbia
e-mail: vcebasek@rgf.bg.ac.rs

Introduction

The portion of the Pan-European Corridor X that crosses Serbia, approximately 90 km, between the city of Nis and the border crossing with Bulgaria, is currently under construction. On the Dimitrovgrad bypass, the southeasternmost part of the alignment, construction has stopped after completion of almost all of the earthworks due to bankruptcy of the contractor. Along the 9 km long section, the design called for the construction of seven bridges, two tunnels, two reinforced earth structures, six retaining walls and a 3 km-long section of cuts over 30 m high (Fig. 1). The terrain mainly comprises flysch deposits represented by a sequence of sandstones and siltstones (occasionally limestone).

The E80 highway investigations were the first detailed site investigations of this part of Serbia. In the flysch area, 22 boreholes were executed, with laboratory tests performed on 16 samples. During the execution of the works, several road cuts suffered from circular failures and

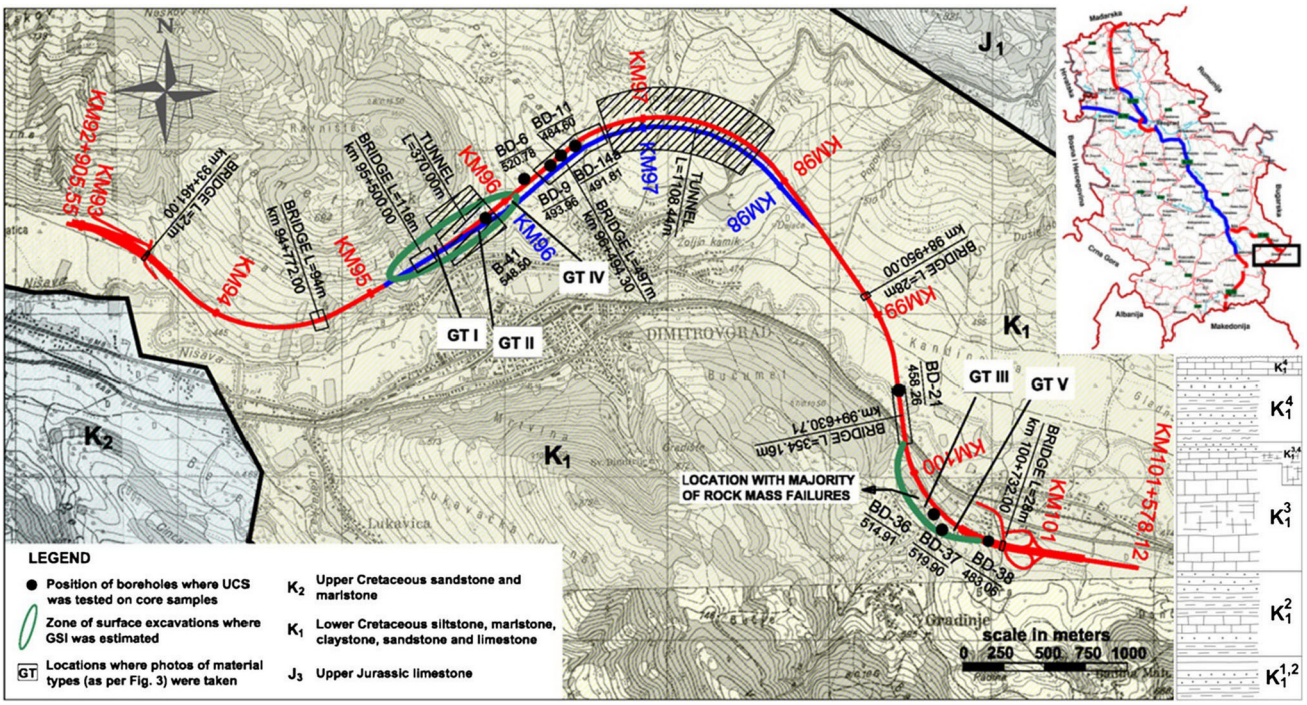

Fig. 1 Location of the study area overlaid on a schematic geologic map with a stratigraphic column

structural instabilities. These failures led to many problems requiring re-design of one part of the cuts. For this purpose, a GSI index was estimated and observations were made of the structural features of the rock discontinuities on the faces of the surface excavations.

Special emphasis in this study is placed on determining the shear strength parameters of flysch by means of an hyperbolic nonlinear failure envelope. A range of possible values is given to parameters which are then verified based on back-analysis of failed slopes. The effect of the non-linearity of strength envelope on the final result is also examined.

Flysch of southeastern Serbia

Flysch deposits are common in southeastern, central and western parts of Serbia. Approximately 15 % of the 250 km of highways under construction will be built in flysch. Flysch consists of a sequence of clastic sediments represented by coarse-grained and fine-grained (clay-bearing/pelitic) sediments. In a sequence deposited in a deep marine environment, adjacent to a rising mountain belt, limestones, sandstones, conglomerates and clay-bearing rocks (siltstones, mudstones, claystone, marls and shales) are usually alternating. The thickness of the individual beds ranges from cm to m, with the flysch sequence having an overall thickness of a few 100 to a few 1,000 m. During the formation of a mountain belt (orogenesis) flysch sediments are exposed to high tectonic pressures leading to alterations, faulting and folding of the original constituents. As a result, normal and reverse faults and thrusts are observed, along with degradation of the rock mass quality. Thus, the quality of the flysch can vary from undisturbed to sheared, or even chaotic, according to typical engineering scales.

The flysch character of sediments surrounding the town of Dimitrovgrad was determined during work on the geological map of Serbia (Dimitrijević et al. 1977).

Flysch sediments of the Dimitrovgrad area belong to the "Timok" tectonic unit, surrounded by the "Stara Planina" unit from the northeast and the "Rtanj-Kucaj" unit from the southwest. The Timok tectonic unit represents a trench structure over 40 km long formed along regional dislocations oriented NNW–SSE. The trench structure is characterized by longitudinal dislocations oriented NW–SE, combined with numerous transversal faults and folds resulting in a complex structure. The flysch deposits are approximately 200 m thick, represented by an alternation of yellowish to bluish sandstone and yellowish siltstone/marlstone (occasionally limestone), interchanging in different proportions. Based on paleontological evidence, the flysch was determined to be of the Lower Cretaceous epoch. A schematic geologic map and a stratigraphic column of alternating units is shown in Fig. 1. Tectonic activity has produced different degrees of disturbance and variability of

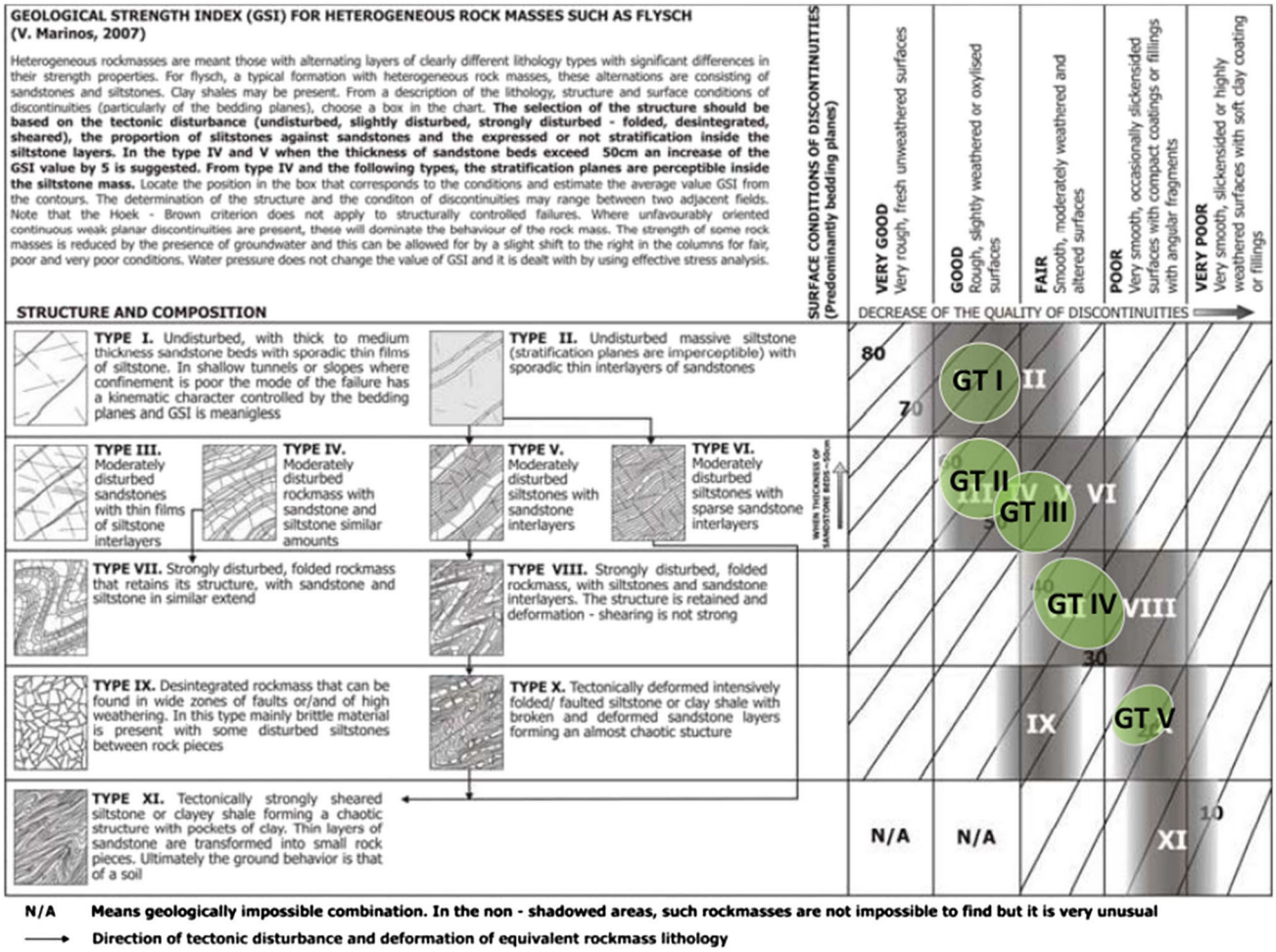

Fig. 2 GSI classification chart for flysch rock mass

the physical and mechanical properties of the rock mass. The flysch quality changes in both the vertical and horizontal direction, usually in the range of a few tens of m.

Laboratory test results on intact rock samples showed that the uniaxial compressive strength (USC) of all the tested samples varies between 10.59 and 70.06 MPa. The bulk density varies between 24.57 and 26.86 kN/m^3.

Application of the GSI for flysch characterization

The GSI classification system is one of the most common tools used to characterize rock mass known as Hoek–Brown material. The GSI was introduced by Hoek (1994) and Hoek et al. (1995) in order to overcome the shortcomings of Bieniawski's rock mass rating (RMR) when applied to intensively jointed rock masses. As one of the parameters of the Hoek–Brown failure criterion, the GSI can be determined by visual inspection of core samples, outcrops or tunnel and road cut faces. It is based on the assessment of the lithology, structure and joint surface conditions. The best results are probably obtained if the GSI is determined on the faces of excavated slopes. A detailed review of GSI application and limitations can be found in Marinos et al. (2005). The first application of the GSI for characterization of heterogeneous flysch deposits was made by Marinos and Hoek (2001). Since then, it has undergone several modifications in order to include new material types. The latest version, Marinos (2007), is used in this paper. It is worth mentioning that GSI charts have been modified in order to be applicable for the quantification of other rock mass types by Hoek et al. (2005) and Marinos (2006, 2010).

For the purpose of re-design, as necessitated by slope failures, the authors performed detailed GSI classification of over 1,500 m of the open excavation faces. Depending on the sandstone/siltstone ratio, tectonic disturbance and joint surface conditions, five rock mass types (GT I–GT V) and possible GSI ranges were determined (Figs. 2, 3; Table 1).

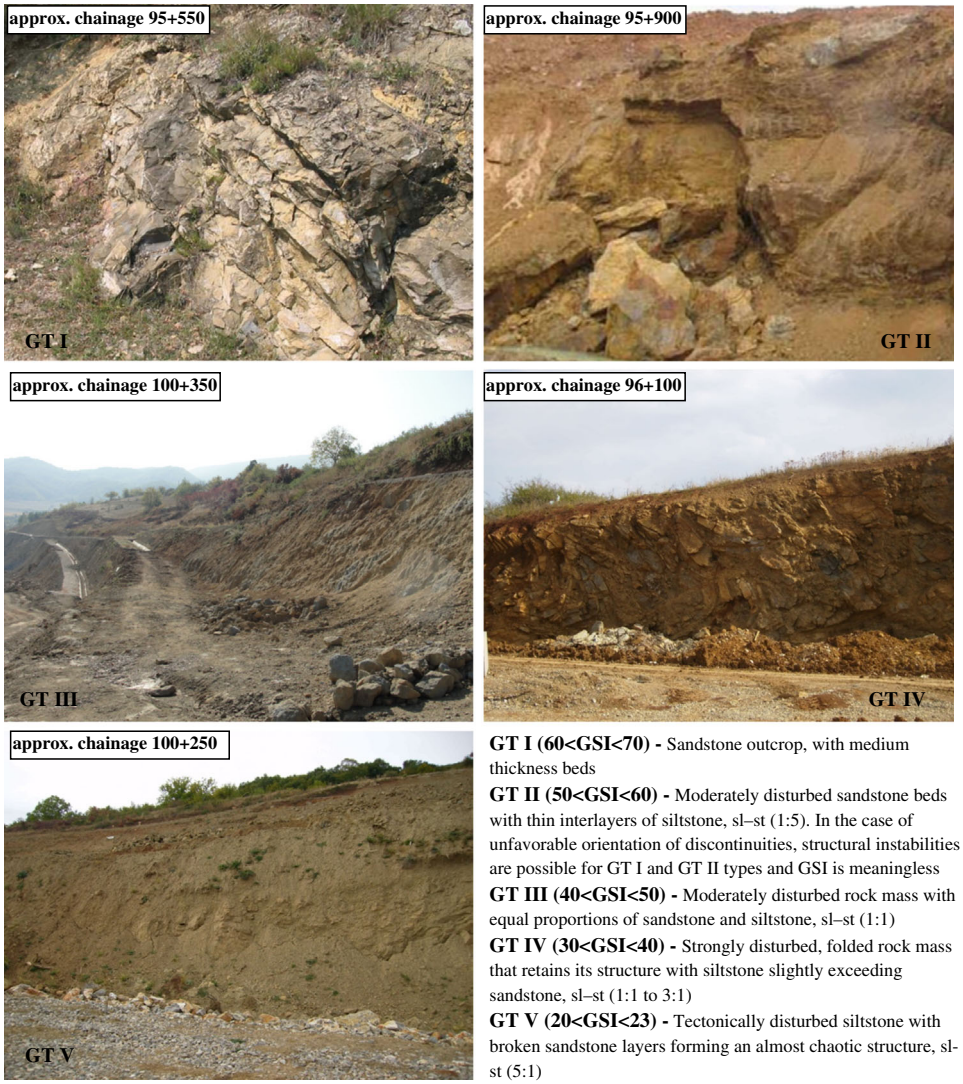

Fig. 3 Typical flysch representatives

Table 1 Geotechnical properties of flysch rock mass

Flysch type on GSI chart	Geotechnical type	Rock mass and intact sample characteristics		
		GSI	σ_{ci} (MPa)	m_i
I	GT I	60–70	60–70	17
III	GT II	50–60	42–47	17
IV	GT III	40–50	27–30	12
VII	GT IV	30–40	18–20	11
X	GT V	20–25	10–12	7–8

Values of petrographic constant m_i are adopted as 7 and 17 for siltstone and sandstone components, respectively, according to suggestions by Hoek and Brown (1997). Pepe et al. (2014), based on data from 95 triaxial tests for the Sanremo flysch formation, obtained m_i values generally higher than those proposed by Hoek and Brown (1997), leading to the conclusion that the most suitable way to determine the petrographic constant m_i is by testing in each particular case.

The intact UCS was determined for 16 laboratory-prepared cylindrical samples (4 siltstone and 12 sandstone samples) according to the 2007 International Society for Rock Mechanics (ISRM 2007) procedure. In order to preserve natural moisture content, samples were wrapped in polyethylene sheets immediately after drilling and kept in such until testing in the laboratory. Sample diameters ranged between 86 and 101 mm, having a height to diameter ratio ranging from 2.5 to 3. In order to take into account the influence of sample size upon rock strength, the compressive strength of a 50 mm-diameter sample was used as a reference, according to Hoek and Brown (1980). Sample depth varied between 3.50 and 32.0 m. Hoek et al. (1998), Marinos (2006) and Hoek and Brown (1997) discussed the practical difficulties associated with determining the σ_{ci} value. The difficulties are mainly related to the

inability to obtain an undisturbed and representative sample characteristic for the entire rock mass. For weaker portions of siltstone material, from which it was impossible to obtain undisturbed samples, lower bound values of the UCS were estimated based on geological hammer blows and partly also on published data in similar ground conditions.

The σ_{ci} value determined was directly applied to GT I material and in all other cases (GT II–GT V) a "weighted average" of the intact UCS was used depending on the siltstone/sandstone ratio.

The m_i value was directly applied to GT I material and, in the case of GT II material (sl–st ratio of 1:5), it was assumed equal to that of a sandstone due to somewhat higher values obtained by Pepe et al. (2014). In all other cases (GT III–GT V) a weighted average of the m_i values were used.

Results of extensive research on the influence of the siltstone percentage (S/P or sl–st ratio) on the mechanical properties of a rock mass were published by Zainab et al. (2007), Budetta and Nappi (2011) and Tziallas et al. (2013). Tziallas et al. tested composite samples with different sl–st ratios and determined that σ_{ci} exponentially decreases with increase in the siltstone percentage. When this ratio exceeds 37 %, σ_{ci} corresponds to the strength of an intact siltstone specimen. In the same study, significant decrease of the m_i parameter for a siltstone percentage of only 17 % was shown based on triaxial compressive test results. On the other hand, Zainab et al. showed that for only 10 % of shale thickness σ_{ci} decreased drastically and that an additional increase in the thickness does not result in much change in composite (shale-sandstone) sample strength. An explanation for the differences in the two studies can be given by the ratio of the compressive strength of the original materials. As this ratio $\left(\sigma_{ci}^{strong}/\sigma_{ci}^{weak}\right)$ increases, the strength of the composite sample decreases more rapidly with an increasing percentage of low-strength material. These facts, along with suggestions of Marinos and Hoek (2001), modified after Marinos (2010), have been considered when determining weighted average intact strength properties.

Determination of shear strength parameters

Shear strength parameters were determined for each rock mass type, according to three failure criteria: the Hoek–Brown (HB) criterion (Hoek et al. 2002); the Mohr–Coulomb (MC) criterion; and a hyperbolic nonlinear envelope (Maksimovic 1979).

HB parameters are derived from collected field and laboratory data in the commercially available software package RocLab (Rocscience Inc 2013). The equivalent MC parameters are obtained by a linear regression method (Hoek and Brown 1997; Hoek et al. 2002) in the same software package.

The Levenberg–Marquardt algorithm (LMA), implemented in the software package KaleidaGraph (Synergy Software 2013) is used for conversion of HB parameters to an hyperbolic envelope. The LMA technique is used for solving nonlinear least squares problems, where the relationship between the dependent and independent variables is given by a nonlinear function. A comprehensive study on fitting experimental data to the HB failure criterion was done by Sari (2012). In this study, a comparison is made between several curve fitting techniques (LMA among them), where both tensile and compressive strengths are utilized.

In the present study, the curve fitting is done for predefined data points of the HB failure envelope by excluding the tensile part of the envelopes. The first step in this process assumes conversion of the HB criterion, defined in principal stress space, to a shear-normal stress function, according to the equations published by Balmer (1952). For such a defined (σ_n, τ) pairs, the best fit is performed with an hyperbolic equation:

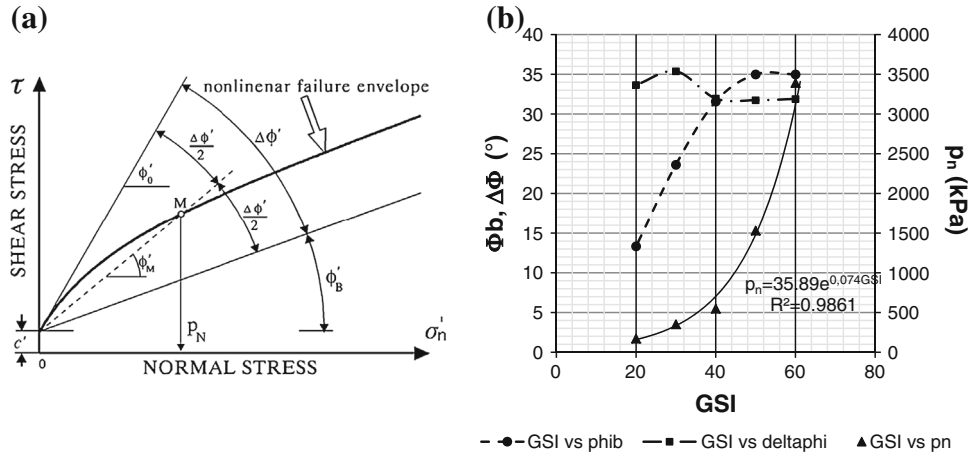

Fig. 4 **a** parameters of the nonlinear failure envelope; **b** variation of p_n, Φ_b and $\Delta\Phi$ with GSI

Table 2 Parameters derived for lower bound values given in Table 1

$H = 20$ m	HB criteron $\sigma_1 = \sigma_3 + \sigma_{ci}(m_b\sigma_3/\sigma_{ci} + s)^a$	MC criteron $\tau = c + \sigma_n \tan\varphi$	Hyperbolic envelope $\tau = c + \sigma_n \cdot \tan(\Phi_b + \Delta\Phi/(1 + \sigma_n/p_n))$	Goodness of fit for hyperbolic envelope		
				Chi square (χ^2)	Coefficient of det. (R^2)	SEV (Φ_b, $\Delta\Phi$, p_n) respectively
GT I	$m_b = 1.887$; $s = 0.003$;	$c = 461.6$ kPa;	$c = 341.17$ kPa; $\Phi_b = 46.46°$; $\Delta\Phi = 21.63°$;	1.80e−10	1	±7.83e−6 ±5.88e−6
$\sigma_{3max} = 493.2$ kPa	$a = 0.503$	$\varphi = 57.8°$	$p_n = 1{,}496.66$ kPa			±1.34e−3
GT II	$m_b = 1.089$; $s = 0.0007$;	$c = 242.8$ kPa;	$c = 104.76$ kPa; $\Phi_b = 41.98°$; $\Delta\Phi = 26.16°$;	4.56e−12	1	±9.29e−7 ±5.64e−7
$\sigma_{3max} = 464.8$ kPa	$a = 0.505$	$\varphi = 52.3°$	$p_n = 868.68$ kPa			±9.47e−5
GT III	$m_b = 0.444$; $s = 0.0002$;	$c = 133.8$ kPa;	$c = 34.34$ kPa; $\Phi_b = 31.58°$; $\Delta\Phi = 31.95°$;	2.32e−14	1	±9.04e−8 ±4.54e−8
$\sigma_{3max} = 427.5$ kPa	$a = 0.511$	$\varphi = 41.8°$	$p_n = 549.74$ kPa			±5.65e−6
GT IV	$m_b = 0.235$; $s = 0.0000392$;	$c = 80.5$ kPa;	$c = 9.89$ kPa; $\Phi_b = 23.62°$; $\Delta\Phi = 35.39°$;	1.17e−13	1	±2.54e−7 ±1.29e−7
$\sigma_{3max} = 397.9$ kPa	$a = 0.522$	$\varphi = 32.7°$	$p_n = 352.42$ kPa			±1.12e−5
GT V	$m_b = 0.0863$; $s = 0.0000092$;	$c = 35.7$ kPa;	$c = 2.59$ kPa; $\Phi_b = 13.34°$; $\Delta\Phi = 33.65°$;	7.36e−15	1	±8.63e−8 ±1.19e−7
$\sigma_{3max} = 355.1$ kPa	$a = 0.543$	$\varphi = 19.5°$	$p_n = 171.46$ kPa			±2.89e−6

$$\tau = c + \sigma_n \tan(\Phi b + \Delta\Phi/(1 + \sigma_n/p_n)) \quad (1)$$

where Φ_b, $\Delta\Phi$ and p_n are parameters having a physical meaning. Φ_b is the basic angle of friction, i.e., the angle of the shearing resistance mobilized at high normal stress levels at which all dilatancy effects are suppressed and shearing takes place on a smooth shearing plane; $\Delta\Phi$ is the maximum angle difference that reflects density, angularity and associated dilatancy effects at zero stress level. In the case of HB material (Hoek and Brown 1997), it could be described as the angle of maximum dilatancy; p_n is the median angle pressure mainly reflecting the strength or the resistance of grains (intact rock pieces in the case of HB material) to crushing.

These parameters are described for coarse- and fine-grained materials and for rough rock joints (Maksimovic 1989a, b, c, 1992). In the case of HB material, the description is practically the same as for coarse-grained soils, except for the addition of cohesion term (c). The geometrical meaning of each parameter is shown in Fig. 4a.

At the beginning of the procedure, it is necessary to enter the initial values of Φ_b, $\Delta\Phi$ and p_n, and then the software iteratively calculates the chi square value (representing the sum of the squared error between the original data and the calculated fit) for which the best fit curve is obtained. The LMA finds only a local minimum, which is not necessarily the global minimum. The global minimum is usually obtained after a few attempts, by successively entering different parameter starting values. The curve fitting is done for three points with one additional point chosen to contain the identical value of the cohesion intercept, i.e., the shear resistance of the rock mass for zero normal stress. Maksimovic (2013) solved the three points conversion problem by reducing the solution to the system of three linear equations in the three variables. In this case, the equivalent parameters of the hyperbolic envelope are dependent on selected points. In order to test the sensitivity of the solution against the number and position of the points, the authors performed a number of calculations (varying between 500 and 3 points) and determined that the best results are obtained for equidistant spacing between the points $(\sigma n, \tau)_{1/9\sigma 3max}(\sigma n, \tau)_{1/3\sigma 3max}, (\sigma n, \tau)_{\sigma 3max}$, which is in agreement with Maksimovic's conclusions. In this way, the error (in the form of chi square, correlation coefficient and standard error values (SEV) of the parameters) is negligibly small or equal to zero, as shown in Table 2. The error values indicate how well the calculated curve fits the original data. The standard errors of the parameters should be read as: parameter value ±error. Equivalent MC and hyperbolic parameters are dependent on the range of minor principal stress chosen, i.e., the maximum value of the minor principal stress (σ_{3max}). The

Table 3 Characteristics of rock discontinuities

Project: Highway E-80 (Dimitrovgrad bypass)										
Chainage: 99 + 812.45 − 100 + 589.52					Rock type: sandstone and siltstone (flysch formation)					
Slope orientation dip direction/dip: 35 (40)/45 (60)					Magnetic declination: 5°					
1 No.	2 Discontinuity type	3 Dip direction (°)	4 Dip (°)	5 Spacing (cm)	6 Persistence (m)	7 Aperture (cm)	8 Roughness	9 Filling material	10 Weathering	11 Comment
1	B	28	35	30–100	1–2	1–3	SM	No	MW–HW	Failure
2	B	40	35	30–100	1–2	1–3	SM	No	MW–HW	Failure
3	B	60	30	30–100	1–2	1–3	SM	No	MW–HW	
4	B	41	24	30–100	1–2	1–3	SM	No	MW–HW	
5	J1	195	88	50–100	1–2	1–3	SM	No	MW–HW	
6	J1	192	68	50–100	1–2	1–3	SM	No	MW–HW	
7	J1	203	77	50–100	1–2	1–3	SM	No	MW–HW	
8	J2	125	42	30–100	<1	2	SM	No	MW–HW	
9	B	33	35	30–100	1–2	2–3	SM	No	MW–HW	Failure
10	J1	210	80	50–100	1–2	1–3	SM	No	MW–HW	
11	J2	115	15	30–100	<1	3–5	SM	Clay	MW–HW	
12	J2	120	20	30–100	<1	3–5	SM	Clay	MW–HW	
13	J2	121	34	30–100	<1	3–5	SM	Clay	MW–HW	
14	B	310	20	5–20	>2	No	SM	No	UW–SW	
15	B	315	10	5–20	>2	No	SM	No	UW–SW	
16	B	310	12	5–20	>2	No	SM	No	UW–SW	
17	B	307	18	5–20	>2	No	SM	No	UW–SW	
18	J3	255	45	30–50	1–3	3–5	SM	No	MW–HW	
19	J3	252	41	30–50	1–3	3–5	SM	No	MW–HW	
20	J3	247	38	30–50	1–3	3–5	SM	No	MW–HW	
21	J3	250	46	30–50	1–3	3–5	SM	No	MW–HW	
22	B	320	10	5–20	>3	No	SM	No	UW–SW	
23	B	310	26	5–20	>3	No	SM	No	UW–SW	
24	B	310	14	5–20	>3	No	SM	No	UW–SW	
25	J1	195	70	50–100	1–2	3–5	SM	Clay	MW–HW	
26	B	20	27	30–100	1–2	1–3	SM	No	MW–HW	
27	B	40	15	30–100	1–2	1–3	SM	No	MW–HW	
28	J3	285	82	30–50	1–3	3–5	SM	No	MW–HW	
29	J3	274	60	30–50	1–3	3–5	SM	No	MW–HW	
30	J2	114	17	30–100	<1	3–5	SM	No	MW–HW	
31	Ji	10	80	/	1–2	5–10	SR	No	MW–HW	
32	B	41	30	30–100	1–2	1–3	SM	No	MW	
33	B	61	57	>100	1–3	1–2	SM–SL	No	SW	
34	B	76	24	30–100	1–2	3–5	SM	No	MW–HW	
35	B	83	31	30–100	1–2	1–3	SM	No	SW	
36	B	320	40	5–20	>3	No	SM	No	UW–SW	
37	J1	207	43	50–100	1–2	1–3	SM	No	SW	
38	B	291	44	5–20	>3	No	SM	No	UW–SW	
39	B	83	38	30–100	1–2	1–3	SM	No	SW	
40	J1	202	73	50–100	1–2	1–3	SM	No	HW	
41	B	340	4	5–20	>3	No	SM	No	UW–SW	
42	B	342	5	5–20	>3	No	SM	No	UW–SW	
43	B	335	7	5–20	>3	No	SM	No	UW–SW	

Table 3 continued

Project: Highway E-80 (Dimitrovgrad bypass)										
Chainage: 99 + 812.45 − 100 + 589.52					Rock type: sandstone and siltstone (flysch formation)					
Slope orientation dip direction/dip: 35 (40)/45 (60)					Magnetic declination: 5°					
1 No.	2 Discontinuity type	3 Dip direction (°)	4 Dip (°)	5 Spacing (cm)	6 Persistence (m)	7 Aperture (cm)	8 Roughness	9 Filling material	10 Weathering	11 Comment
44	B	64	57	>100	1–3	1–2	SL	No	MW–HW	
45	B	60	62	>100	1–3	1–2	SL	No	MW–HW	
46	Ji	155	70	/	1–2	2–3	SM	No	MW–HW	

2 *B* Bedding plane, *J* Joint, *Ji* Individual joint

5 Distance between adjacent discontinuities

6 Internal length of discontinuities (into the rock mass)

8 *VR* very rough, *R* rough, *SR* slightly rough, *SM* smooth, *SL* slickensided

10 *UW* Unweathered, *SW* slightly weathered, *MW* moderately weathered, *HW* highly weathered, *D* decomposed

value of $\sigma_{3\max}$, which is a function of slope height, unit weight and rock mass strength, was determined according to Hoek et al. (2002). This paper considers cuttings 20 m high.

The excavation is mainly performed by mechanical means, with blasting to a lesser extent. The average measured discontinuity aperture ranges from 1 to 5 cm (Table 3), indicating the influence of stress relief due to overburden removal; thus, the disturbance factor is adopted to be $D = 0.7$.

Table 2 shows parameters determined according to the abovementioned procedures.

From Table 2 it can be seen that the basic friction angles are unrealistically high for the GT I and GT II material types. The value of Φ_b is dependent on the moisture condition of the test specimen and can be determined from a suitable laboratory test or assumed from published papers and tables (e.g. Barton 1973; Patton 1966; Ripley 1962; Krsmanovic 1967; Coulson 1972). The value of Φ_b is chosen to be equal to 35°. For such a defined basic friction angle, the maximum angle difference and the median angle pressure for GT I and GT II types are: $\Delta\Phi = 31.9°$, $p_n = 3{,}392.56$ kPa and $\Delta\Phi = 31.74°$, $p_n = 1{,}532.96$ kPa, respectively. Figure 4b shows hyperbolic envelope parameter variation with the GSI. Parameter p_n exponentially increases with an increased GSI, Φ_b decreases with the GSI, while the maximum angle difference is obtained for GSI = 30. The variation of $\Delta\Phi$ could be described by the fact that for lower GSI values the overall quality of the rock mass is reduced, leading to easier crushing of rock fragments. On the other hand, for higher GSI values failure involving discontinuity surfaces, rather than by fragment rotation and interlocking, could be more critical.

Verification of parameters

Verification of the proposed parameters is based on back-analysis of failed slopes. The majority of failures happened between ch 99 + 800 and ch 100 + 600.

In the case of cuttings excavated in GT I and GT II materials, structural instabilities represent the dominant failure mode. Analysis of planar failure in GT II material allowed for verification of the previously adopted value of the basic angle of friction Φ_b. In order to discuss possible failure modes in GT I and GT II materials in more detail, stereonet plots of structural data were analyzed.

The median angle pressure values (Table 2) are compared with published data.

For slopes excavated in the GT III and GT IV categories, problems with instabilities were not observed.

The major problem is excavation in GT V material where, soon after completion of the cuttings, global failures occurred (Fig. 5b, d). The proposed set of parameters for the GT V material was verified based on back-calculations of the failed slope with a circular sliding surface.

Analysis of structural data and verification of Φ_b and p_n

When plotted on stereonet diagrams the orientation of discontinuity planes (as per Table 3) show the relative scatter of the data (Fig. 6). Three joint sets J1, J2 and J3, bedding planes B (oriented in two directions due to folding) and random joint Ji are distinguished. The mean plane orientations of sets J1, J2, J3 and the bedding planes are: 206/69; 125/26; 262/46; 55/28 and 316/17, respectively.

Wedge, planar and toppling (flexural and direct) analyses were performed to determine the failure probability of each instability mode according to the procedure described

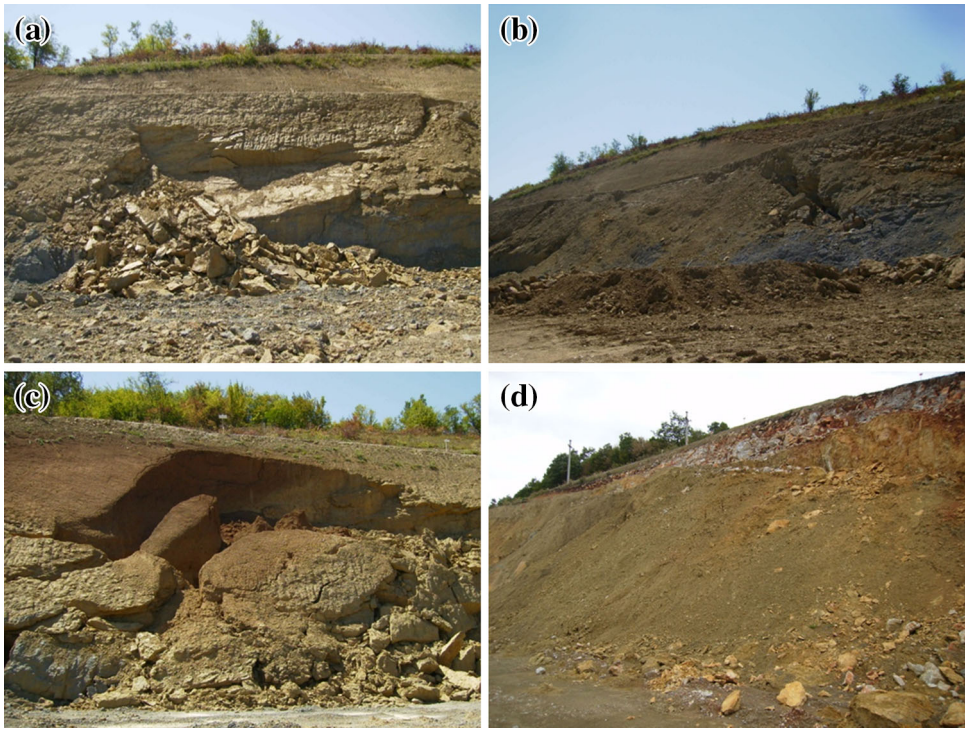

Fig. 5 Typical failures in flysch material. **a** Planar failure in GT II material; **b** global (circular) failure in GT V material; **c** failure at the soil and GT V material contact; **d** failure in extremely sheared siltstone (soil like material) located in the overthrust zone

in Hudson et al. (1997). These analyses were performed using the software package Dips (Rocscience Inc 2014); results are shown in Fig. 6a–d.

As can be seen from Fig. 6a, the overall probability of planar sliding is relatively small, but highly possible (approx. 30 %) for the bedding plane with a mean plane orientation of 55/28 (set 1). According to the characteristics of discontinuities (Table 3), all the rock surfaces are smooth enough (occasionally slickensided) to assume that no surface roughness would affect the Φ_b value. In the case of planar failure as shown in Fig. 5a, dip elements (28/35) led to the conclusion that for the reasonably assumed zero cohesion between discontinuity surfaces and the existence of a release plane, the basic angle of friction is equal to 35°.

Five mean discontinuity planes intersect each other to form 10 intersection points, but none of them are within the critical wedge sliding zone, leading to the conclusion that wedge sliding is not a major issue for this slope orientation. The overall wedge failure probability is approx. 5 % (Fig. 6b).

The possibility of flexural toppling is very small (approx. 2 %), but for direct toppling it is relatively high in respect to discontinuity orientation (Fig. 6c–d). Toppling combined with sliding of blocks is indeed observed (Fig. 7).

Maksimovic (1996) presented typical median angle pressures for some soil types, as shown in Table 4. From comparison with values obtained for the five flysch types of southeastern Serbia, it can be concluded that the p_n values are widely distributed. The lower bound value of 170 kPa corresponds to fine-grained soils, while the upper bound value corresponds to well-graded gravel and angular rockfill. This wide range of values is logical, bearing in mind the different degrees of disturbance of the rock mass due to intense tectonic activity. The more the rock mass is tectonically disturbed, the larger the percentage of pelitic components, thus providing a lower p_n.

Global failures and verification of parameters for GT V material

In order to check the validity of the proposed parameters for GT V material, back-analysis is performed on the failed slopes, as shown in Fig. 5b.

The landslides in GT V material are similar in nature and have the same prevailing failure mechanism and dimensions. They are usually 2–3 m thick, extending from the crest to the toe of the individual benches. All slopes have been excavated in dry conditions, prior to the rainfall season.

According to site documentation, the excavation in the wider zone of the slope started in June 2011 and reached the designed elevation in August. After finishing the excavation, wetting on the face of the slope was noticed due to intensive rainfall and the existing water catchment located several meters behind the crest of the slope. This led to an increase in pore-water pressure in the slope. The

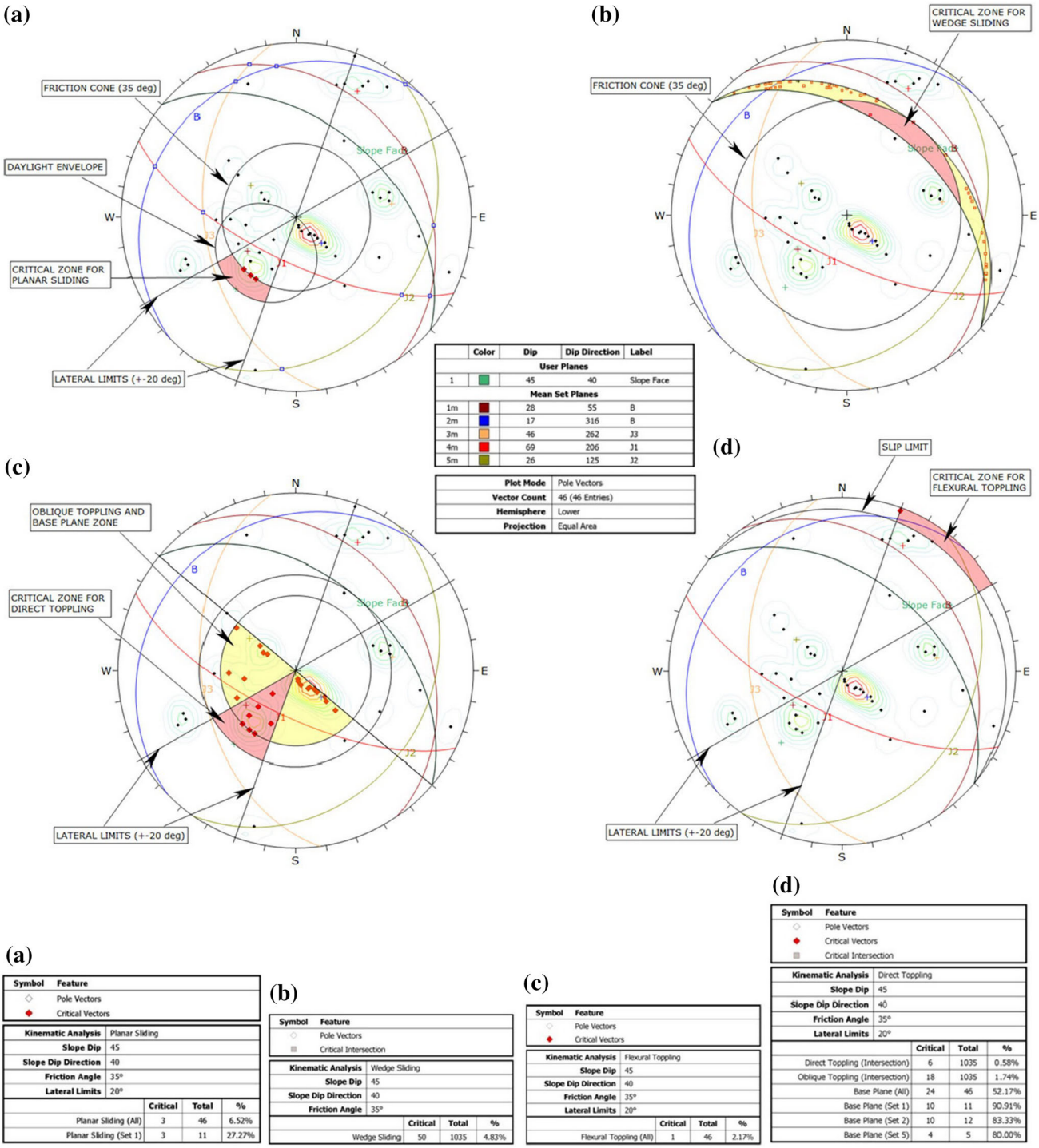

Fig. 6 Analysis of different failure modes. **a** Planar sliding; **b** wedge sliding; **c** direct toppling; **d** flexural toppling with legend corresponding to each failure mode

collapse occurred in October 2011. When dealing with cut slopes excavated in flysch, a certain degree of slaking of clay-bearing rocks can be expected. The slaking phenomenon, i.e., disintegration due to heating and cooling, wetting and drying and freezing and thawing effects, has been investigated by many researchers (Botts 1998; Santi and Higgins 1998; Gokceogly et al. 2000; Picarelli et al. 2006; Hoek et al. 2005; Miscevic and Vlastelica 2011; Miscevic and Vlastelica 2014; Gautam and Shakoor 2013). The rate and amount of slaking depends on the type of clay-bearing

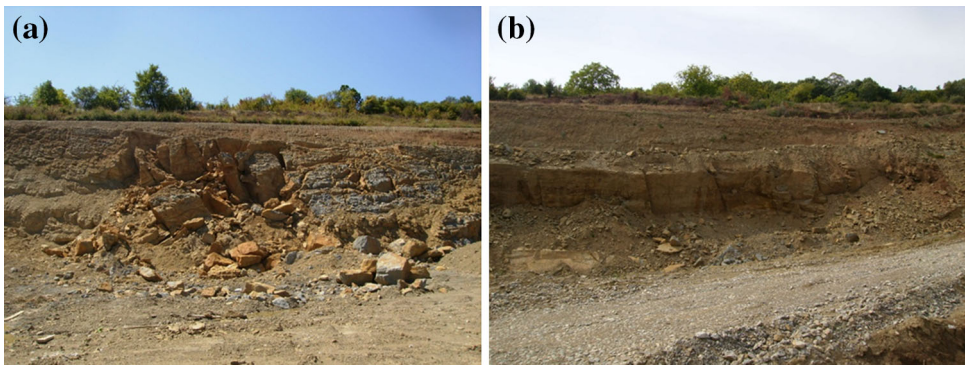

Fig. 7 **a** Toppling failure combined with block sliding in GT II material; **b** blocks with toppling potential

Table 4 Median angle pressure p_n for different materials (Maksimovic 1996)

Material type	p_n (kPa)
Clays	20–150
Anthracite	100
Calc. sands	250–400
Silicia sands	300–700
Angular rockfill	350–2,000
Well graded gravel	500–4,000
Al. oxide	10,000
Dimitrovgrad flysch (GT V–GT I)	170 (230[a])–3,400 (6,630[a])

[a] Exact upper bound values of median angle pressure for GT V and GT I materials (given the range of values in Table 1) are 233.80 and 6,631 kPa, respectively. The basic angle of friction was assumed as 35° for GT I material

rock and climatic conditions of the region. In order to slake, material needs to be totally or partially dried and then rewetted (Botts 1998). Slaked material tends to transgress from rock-like to soil-like material, which leads to reduction of shear strength. As the time between completion of the slopes and failure was only 2 months and wetting of the toe was observed just after completion of the excavation, the slaking process was not likely to develop and could not have any major influence on the global stability of the slope.

The geometry of the slope is shown in Fig. 8. The inclination of the lower slope is 45° and the height is 12 m. The upper slope is 7.5 m high and inclined to 40°. The width of the intermediate bench is 2 m.

Bishop's simplified method was used to perform slope stability analyses, since the observed failure surface is of a circular type. Calculations were performed by assuming plane strain conditions in the software packages Slide and BGSlope. Both packages allow a choice of several shear strength criteria for performing slope stability analyses. Factors of safety in Slide were calculated by assuming the MC and HB criterion and in BGSlope by assuming the MC and hyperbolic criterion.

The first analyses were performed in dry conditions, as this was the actual situation prior to slope failure. A safety factor of FoS = 1.15 is obtained for the HB and hyperbolic envelope. For the MC criterion the safety factor equals 1.19 (Fig. 8a).

Subsequent analysis was performed with an average pore-water pressure ratio $r_u = 0.1$ acting on the slope. This means that the slope is approx. 20 % saturated, a common assumption in slope stability analyses when dealing with this kind of material. In this case, the obtained FoS = 1 for HB and the hyperbolic envelope indicates failure (Fig. 8b). The critical failure surface extends from the toe to the crest of the lower bench, and corresponds to the actual sliding surface (Fig. 5b). The sliding surface is between 2.5 and 3.0 m thick, resulting in a maximum effective normal stress in the range 50–55 kPa (Fig. 9a). When discussing stresses it is worth nothing that stress is a tensor quantity defined by the magnitude, direction and orientation of the planes on which the stress components are acting. The in situ stress state is altered when excavating a slope, resulting in a change in principal stress orientation and magnitude. Stress state is also influenced by rock anisotropy and discontinuity leading to the expectations that values of in situ stresses are likely to be variable. Thus, it can be concluded that in situ stresses are very difficult to determine/estimate and even when a stress estimation strategy is made one cannot entirely rely on stress estimation results. Moreover, in rock materials up to a certain depths horizontal stresses are usually higher than the vertical ones. This is mainly to do with tectonic movements and overburden removal. The higher the ratio of horizontal to vertical stress (K_0) the larger displacements of the slope can be expected upon excavation. This paper deals with the limit equilibrium method of slices (LEM) based on conditions of static equilibrium; thus, computed stresses do not necessarily represent actual field conditions. A better approach is to determine stresses using the stress–strain finite element method (FEM) that ensures displacement compatibility.

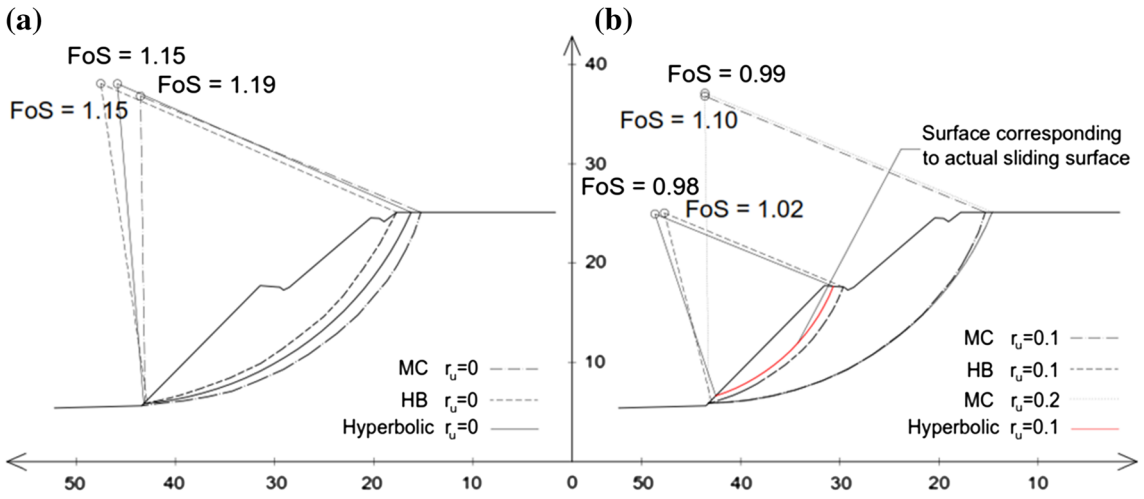

Fig. 8 Results of slope stability analyses

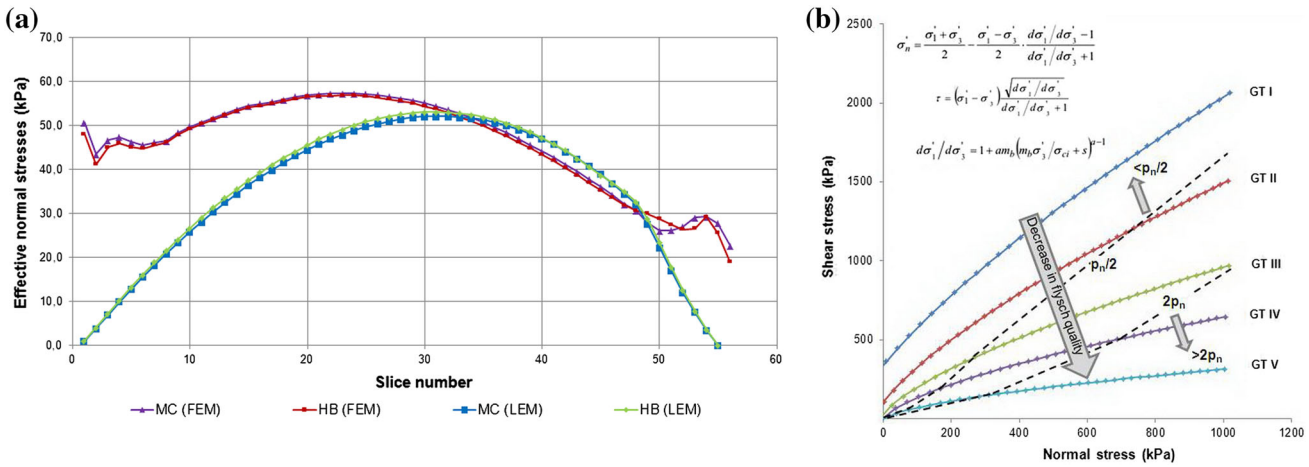

Fig. 9 **a** Effective normal stresses computed by FEM and LEM; **b** σ_n–τ envelopes for Dimitrovgrad flysch showing a decrease in rock mass quality

In order to use the FEM stresses in an LEM framework, the procedure proposed by Krahn (2003) was utilized. In the first step, in situ stresses were calculated by the gravity turn-on technique in the software package Sigma/W. The computed stresses were then used to calculate normal stresses along the slip surface (for MC and HB criteria) in the software package Slope/W. Stress history was not considered in the FEM analyses. The unstructured mesh was generated by 2,582 6-noded triangular finite elements and material properties were represented by an elastic–plastic constitutive model with the MC failure criterion. Deformation parameters of the constitutive model E and v are adopted to be 20,000 kPa and 0.3, respectively. It can be readily shown that the Young's modulus does not have any influence on computed stresses while the value of Poisson's ratio influences distribution of FEM stresses, but the maximum magnitudes vary only slightly (±5 kPa).

The normal stress distribution along the slip surface is shown on Fig. 9a. It can be seen that the stresses calculated by the two methods differ but the maximum expected magnitudes are quite similar and may be treated as the same for practical applications. Whether stresses are computed by FEM or LEM they need not to be representative of in situ conditions due to uncertainties related to geological process that created the slope. For the purpose of further discussion the authors have decided to conform to the results of the LEM because it is shown that the LEM realistically represents in situ conditions regarding the position of the sliding surface and the safety factor value.

By introducing the pore pressure ratio the effective normal stresses acting on a sliding surface are reduced, thus transferring the shear strength to the curved part of the envelope. The curvature intensity of the failure

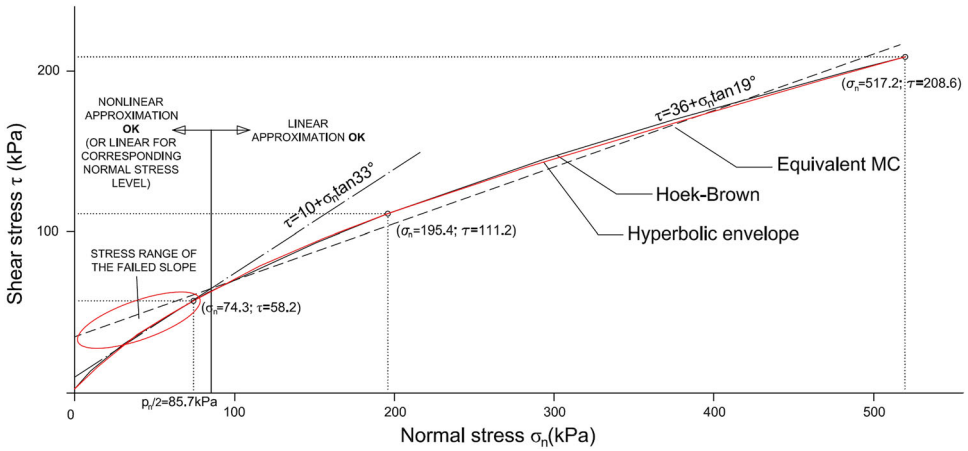

Fig. 10 Effect of nonlinearity on shear strength of the failed slope

envelope can be expressed in terms of the stress level ratio (Maksimovic 1996), which is the ratio of normal effective stress and median angle pressure (SLR $= \sigma_n/p_n$). Based on the SLR concept, the strength envelope can be divided into three segments: SLR < 0.5 (high curvature); $0.5 <$ SLR < 2 (transitional curvature); and SLR > 2 (straight line). In the case under consideration, the SLR is 0.32, leading to the conclusion that the curvature of the envelope is highly pronounced and has to be properly considered in the analyses. Figure 9b shows the shear strength envelopes for the five GT materials plotted in σ_n–τ space up to a normal stress of 1,000 kPa. The dashed borderlines intersect the strength envelopes in the points having the values of $p_n/2$ and $2p_n$. This kind of presentation could be useful if one wants to determine whether the value of the normal stress acting on the sliding surface in one of the GT materials is critical for considering the curvature of the failure envelope in the analysis. In the case of the MC criterion, the critical sliding surface encompasses the entire slope with a safety factor FoS $= 1.10$. The linear envelope overestimates shearing strength in the low normal stress range, which could lead to the conclusion that the slope is virtually stable. In order to reach a state of failure (FoS $= 1$) in the case of the MC criterion, the subsequent analysis was performed by assuming $r_u = 0.2$. In this case, the sliding surface encompasses the entire slope and is slightly shifted towards the back of the slope, which does not correspond to the actual sliding surface.

In the presented case, it would be more appropriate to consider a different set of linear parameters in the stress range of interest (Fig. 10). In this particular problem, with up to 85 kPa (SLR < 0.5), the linear parameters that best describe the curved part of the envelope are $c = 10$ kPa and $\Phi = 33°$. With this set of parameters and $r_u = 0.1$, the same results are obtained as for the initially-assumed nonlinear envelope.

Concluding remarks

This paper deals with the shear strength properties of complex flysch rock masses characteristic of southeastern parts of Serbia, particularly in the wider area of Dimitrovgrad close to the border crossing with Bulgaria. The need for flysch characterization arose from several slope failures that occurred just after completion of cuttings on the E80 highway project.

Based on GSI classification, five distinct rock mass types have been defined. For the GT I and GT II types, structural failures are common in the case of unfavorable orientation of discontinuity planes. In the GT V type, global instabilities through the rock mass are observed.

Shear strength parameters are defined for three shear strength criteria: the Hoek–Brown criterion; the Mohr–Coulomb criterion; and a hyperbolic nonlinear envelope.

This is the first time that an hyperbolic envelope has been used to define the shear strength properties of flysch rock mass. Parameters of the hyperbolic envelope are obtained by nonlinear regression, as a best fit of data to the shear-normal function of the Hoek–Brown criterion, using the Levenberg–Marquardt algorithm. Conversion from HB to the hyperbolic criterion is relatively insensitive to the σ_{3max} chosen due to the nonlinear nature of the envelopes.

The equation for conversion of HB to equivalent MC parameters (Hoek et al. 2002) is not suitable when steep slopes with pore pressures are considered, leading to non-conservative results and erroneous positioning of the sliding surface. The reason for this lies in how these equivalent parameters are estimated, which is largely to do with estimating a suitable minor principal stress range. This is in agreement with the conclusions of Li et al. (2008), where for steep (1:1 and steeper) and gentle slopes new equations for estimating the minor principal stress were proposed.

Parameter p_n exponentially increases with an increasing GSI, and ranges between 170 and 6,630 kPa. The lower

bound value of 170 kPa corresponds to fine-grained soils, while the upper bound values correspond to well-graded gravel and angular rockfill. This wide range of values is logical, bearing in mind the different degrees of disturbance of the rock mass due to intense tectonic activity. The more the rock mass is tectonically disturbed, the larger the percentage of pelitic components, thus providing a lower p_n. The maximum angle difference is expected when GSI = 30. The basic angle of friction decreases with a decrease in rock mass quality. As the parameters are the result of the conversion process, it is advisable to determine at least one parameter, i.e., the basic friction angle, from direct measurements.

Parameters are verified based on back-calculation of planar and circular failures. One of the main reasons for global failures in GT V material is an increase in pore-water pressure.

In the case of stress-dependent shear strength, it is possible to obtain good agreement between the calculated and actual failure surface. In the case under consideration, the SLR is around 0.32, leading to the conclusion that the curvature of the envelope is highly pronounced. Assuming a best fit straight line over the entire considered stress range could lead to erroneous results.

References

Balmer G (1952) A general analytical solution for Mohr's envelope. Am Soc Test Mat 52:1260–1271

Barton NR (1973) Review of a new shear strength criterion for rock joints. Eng Geol 7:287–332

Botts M (1998) Effects of slaking on the strength of clay shales: a critical state approach. In: Proceedings of the 2nd international symposium on the geotechnics of hard soils/soft rocks, vol 1, Napples, Italy

Budetta P, Nappi M (2011) Heterogeneous rock mass classification by means of the geological strength index: the San Mauro formation (Cilento, Italy). Bull Eng Geol Environ 70:585–593

Coulson JH (1972) Shear strength of flat surfaces in rock. In: Coridng EJ (ed) Proceedings of the 13th symposium on rock mechanics, Urbana Illinois, pp 77–105

Dimitrijević M, Dragić D, Karamata S, Sikošek B, Veselinović D (1977) Explanatory booklet for the basic geological map of SFR Yugoslavia—Sheet Pirot 1:100 000. Federal geological survey, Belgrade (in Serbian), p 69

Gautam P, Shakoor A (2013) Slaking behavior of clay-bearing rocks during a one-year exposure to natural climatic conditions. Eng Geol 166:17–25

Gokceogly C, Ulusau R, Sonmez H (2000) Factors affecting the durability of selected weak and clay-bearing rocks from Turkey, with particular emphasis on the influence of the number of drying and wetting cycles. Eng Geol 57:215–237

Hoek E (1994) Strength of rock and rock masses. News J ISRM 2(2):4–16

Hoek E, Brown ET (1997) Practical estimates of rock mass strength. Int J Rock Mech Min Sci 34(8):1165–1186

Hoek E, Brown ET (1980) Underground excavations in rock. Institution of Mining and Metallurgy, London, p 527

Hoek E, Kaiser PK, Bawden WF (1995) Support of underground excavations in hard rock. Balkema, Rotterdam

Hoek E, Marinos P, Benissi M (1998) Applicability of the geological strength index (GSI) classification for very weak and sheared rock masses. The case of the Athens Schist Formation. Bull Eng Geol Environ 57(2):151–160

Hoek E, Carranza-Torres CT, Corkum B (2002) Hoek-Brown criterion-2002 edition. In: Proceedings of the NARMS-TAC conference, Toronto, vol 1, pp 267–273

Hoek E, Marinos P, Marinos V (2005) Characterization and engineering properties of tectonically undisturbed but lithologically varied sedimentary rock masses. Int J Rock Mech Min Sci 42(2):277–285

Hudson JA, Harrison JP (1997) Engineering rock mechanics—An introduction to the principles. Pergamon Press, Oxford, p 444

ISRM (2007) The complete ISRM suggested methods for rock characterization, testing and monitoring: 1974-2006. In: Ulusay R, Hudson JA (eds) Suggested methods prepared by the commision on testing methods. International Society for Rock Mechanics Compilation Arranged by the ISRM Turkish National Group Ankara, Turkey

Krahn J (2003) The 2001 R. M. Hardy lecture: the limits of limit equilibrium analyses. Can Geotech J 40:643–660

Krsmanovic D (1967) Initial and residual shear strength of hard rocks. Geotechnique 160:145–160

Li A, Merifield RS, Lyamin AV (2008) Stability charts for rock slopes based on the Hoek-Brown failure criterion. Int J Rock Mech Min Sci 45(5):81–89

Maksimovic M (1979) Limit equilibrium for nonlinear failure envelope and arbitrary slip surface. In: Proceedings of the 3rd Int Conf Num Meths Geomech, Aachen, pp 769–777

Maksimovic M (1989a) Non-linear envelope for soils. J Geotech Eng 115(4):581–586

Maksimovic M (1989b) On the residual shearing strength of clays. Geotechnique 39(2):347–351

Maksimovic M (1989c) Nonlinear failure envelope for coarse-grained soils. In: Proceedings of the 12th Int Conf SMFE, Rio de Janeiro, vol 1, pp 731–734

Maksimovic M (1992) New description of the shear strength for rock joints. Rock Mech Rock Eng Springer 25(4):275–284

Maksimovic M (1996) A family of nonlinear failure envelopes for non-cemented soils and rock discontinuities. Electron J Geotech Eng. http://www.ejge.com/1996/Ppr9607

Maksimovic M (2013) BGSLOPE Slope stability software package for PC

Marinos V (2007) Geotechnical classification and engineering geological behaviour of weak and complex rock masses in tunneling. Doctoral thesis, School of Civil Engineering, Geotechnical Engineering Department, National Technical University of Athens (NTUA), Athens

Marinos V (2010) New proposed GSI classification charts for weak or complex rock masses. Bull Geol Soc Greece XLIII 3:1248–1258

Marinos P, Hoek E (2001) Estimating the geotechnical properties of heterogeneous rock masses such as flysch. Bull Engg Geol Env 60:85–92

Marinos V, Marinos P, Hoek E (2005) The geological Strength index: applications and limitations. Bull Eng Geol Environ 64:55–65

Marinos V, Fortsakis P, Prountzopoulos G (2006) Estimation of rock mass properties of heavily sheared flysch using data from tunnelling construction. In: Proceedings of the 10th IAEG, Nottingham, p 314

Miscevic P, Vlastelica G (2011) Durability characterization of marls from the region of Dalmatia. Croatia Geotech Geol Eng 29:771–781

Miscevic P, Vlastelica G (2014) Impact of weathering on slope stability in soft rock mass. J Rock Mech Geotech Eng 6(3):240–250

Patton FD (1966) Multiple modes of shear failure in rock and related materials. Thesis, University of Illinois

Pepe G, Piazza M, Cevasco A (2014) Geomechanical characterization of a highly heterogeneous flysch rock mass by means of the GSI method. Bull Eng Geol Environ. doi:10.1007/s10064-014-0642-4

Picarelli L, Urciuoli G, Mandolini A, Ramondini M (2006) Softening and instability of natural slopes in highly fissured plastic clay shales. Nat Hazards Earth Syst Sci 6:529–539

Ripley CF, Lee KL (1962) Sliding friction tests on sedimentary rock specimens. Proc Seventh Congress on Large Dams 4:657–671

Rocscience Inc. (2013) Roclab user's guide

Rocscience Inc. (2014) Dips user's guide

Santi P, Higgins J (1998) Methods for predicting shale durability in the field. Geotech Test J 21(3):195–202

Sari M (2012) An improved method of fitting experimental data to the Hoek–Brown failure criterion. Eng Geol 127:27–35

Synergy Software (2013) KaleidaGraph guide

Tziallas GP, Saroglou H, Tsiambao G (2013) Determination of mechanical properties of flysch using laboratory methods. Int J Rock Mech Min Sci 166:81–89

Zainab M, Kamaruzaman M, Cho Gye C (2007) Uniaxial compressive strength of composite rock material with respect to shale thickness ratio and moisture content. Electron J Geotech Eng. http://www.ejge.com/2007/Ppr0755/Ppr0755.pdf